Development and Use of a Saturated Absorption Spectroscopy Cell for Tuning the Frequency of the Atom-Cooling Laser

Michael Peron
Advisor: Dr. Thomas Killian

Abstract

This thesis describes the construction, design, and subsequent successful use of a saturated absorption spectroscopy cell, along with complimentary electronics and temperature control to tune and eventually lock the frequency of the atom-cooling laser. By improving the flexibility of control of the magnetic field within the cell, the design allows cooling of different isotopes of strontium with greater accuracy, along with a more precise lock on the transition frequency desired.

1. INTRODUCTION

1.1 Laser Cooling

Laser cooling requires the excitation of individual atoms from their ground state to an excited state by the absorption of a photon with energy corresponding to the transition. The atoms are heated to a vapor and then slowed by three pairs of orthogonal counter-propagating lasers. Each of the lasers is red-detuned from the atomic transition, so that for an atom moving against the beam, the Doppler-shifted laser drives the transition. The absorption of the photon, along with its momentum, slows down the atom, and the subsequent re-emission of the photon adds a random component to the atom's momentum. Averaging over many such collisions for all six lasers, the atom's momentum decreases to the Doppler limit – the low-temperature boundary of such cooling. In summary, the lasers impart a velocity-dependent force that slows down the atoms in question, achieving an effect known as "optical molasses."

While this process slows down the sample, thereby cooling it, the velocity-dependent force cannot trap the atoms for study. Trapping is achieved by an in-homogenous magnetic field, designed such that there is zero field at the center. As an atom moves away from this center, the magnetic field on the atom increases and induces energy level splitting in the atom by the Zeeman effect. This brings their transition more in resonance with the lasers, eventually causing the same momentum decrease by the photon collision. Thus, the force on the atoms by the lasers increases as the atoms attempt to escape, effectively trapping the cooled sample. This combination of slowing lasers and trapping field is known as a magneto-optical trap.

1.2 Saturated Absorption Spectroscopy

In order for the processes described above to work, the original laser (which is later divided into the six beams) needs to output at a single frequency with minimal variation to

ensure uninterrupted resonance. Even small fluctuations hinder the cooling process and/or allow many atoms to escape the trap. In fact, the threshold for such a problematic fluctuation is so small that a wavemeter is not sufficiently precise to monitor changes; instead, one typically uses a saturated absorption spectroscopy (SAS) cell with complimentary electronics to tune and lock the frequency of the laser on the desired transition. This SAS cell is filled with the same atoms as the main sample (in the same vaporous state) and placed between the source and the main sample so that the frequency of the laser can be locked before reaching the experiment.

Saturated absorption spectroscopy is a specific type of frequency-modulation spectroscopy, or FMS. In a typical set up, a laser shines through a sample of gas and hits a photodiode, which measures the intensity of light passing through the gas. If enough photons interact with the gas, the intensity of the laser reaching the photodiode decreases, giving an absorption dip. Since the laser is being swept through a range of frequencies, the dip corresponds to the frequency of the atomic transition [1].

Unfortunately, this dip is rather wide, due to an effect called Doppler broadening. If the atoms were perfectly still and the laser was tuned to the transition as it shone through, there would be a sharp, precise dip right at the resonant frequency, equal in width to the natural linewidth of the transition. However, the thermal motion of the atoms causes a random distribution of velocities. For a given atom, the component of its velocity parallel to the laser determines at what frequency it “sees” the laser, due to the Doppler effect. Thus a wide distribution of parallel velocities leads to a wide distribution of resonances, broadening the absorption profile.

To combat this problem, a second, much stronger beam is sent nearly counter-propagating to the original beam, with a small overlap of beams within the cell. Because the stronger beam is essentially the reverse of the weak beam, each beam interacts with atoms

going the same parallel velocity but in the opposite direction, via the Doppler effect. This means that for the most part, each beam interacts with separate groups of atoms. At resonance, however, both beams compete for atoms near zero velocity. The stronger beam quickly excites many of these atoms, leaving considerably less in the ground state. To the weak beam, it appears as if there are very few atoms to excite near resonance, so that much more of the original light intensity reaches the photodiode. This appears as a sharp rise near the minimum of the original Doppler-broadened absorption, and gives an accurate location for the frequency of the transition. The sharp rise is called the Lamb Dip, and the overall effect is known as saturation, giving rise to SAS. It should be noted that usually, the strong beam is called the pump beam, while the weak beam is called the probe beam.

Since FMS experiments (and by extension, SAS experiments) rely on measurements of intensity to determine absorption lines, fluctuations of that intensity are responsible for the majority of noise. To clarify our absorption profile, a second weak beam is sent through the cell without crossing the strong beam. Both of these probe beams will experience the same intensity fluctuations, and if their powers are matched, one can simply subtract the beams from each other to clarify all intensity-based noise [1]. With this second beam in place, we have our basic SAS schematic:

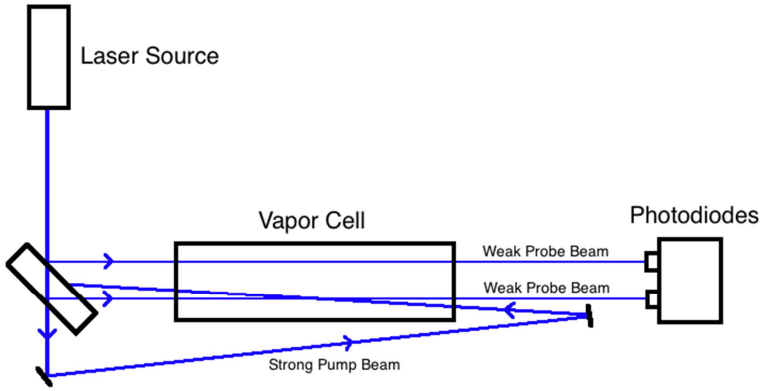

Figure 1.1: Simplified SAS schematic, showing the pump beam crossing one of the probe beams (this is the probe beam with the Lamb Dip). The reflection of the pump beam off the initial mirror is neglected.

1.3 Strontium Isotopes

All laser-cooling experiments in the Killian Lab use strontium at natural abundance, meaning a mixture of naturally occurring isotopes. For strontium in particular, this represents about 83% Sr^{88}, 10% Sr^{86}, 7% Sr^{87}, along with less than 1% of Sr^{84}. Each isotope has its own excitation frequency, and the difference between these frequencies is small enough to where each peak is hidden within the larger Doppler profile of non-SAS spectroscopy, but also appreciable enough to be measured within this range. For technical reasons beyond this thesis, cooling Sr^{88} is not necessarily desirable for most experiments. However, when we run SAS spectroscopy on a sample of naturally abundant strontium, the overwhelming percentage of Sr^{88} causes the Lamb Dip to center itself about that particular excitation frequency, in turn cooling only Sr^{88} in the magneto-optical trap.

In order to cool the more desirable isotopes, we turn once again to the Zeeman shift. Conducting wire is coiled tightly around the cell in multiple layers to create a solenoid. The strong magnetic field created by running current through the wire Zeeman shifts the transitions of the atoms within the cell. By precisely controlling the strength of the magnetic field, and with prior knowledge of the exact difference between each of the isotopes' respective excitation frequencies, we can shift, for example, the Sr^{88} transition to where the Sr^{87} transition usually lies. When we run our laser through the cell, we still lock on the more abundant Sr^{88} atoms, but at the Sr^{87} excitation frequency. The laser continues to the main experiment, where the transitions aren't shifted, and Sr^{87} is cooled.

1.4 Electronic Locking

Saturated absorption spectroscopy gives the location of the Lamb Dip, but it in no way locks the frequency of the laser on it. This is accomplished through the complimentary electronics, connected to both the cell and the laser itself, providing a sort of feedback loop. While this particular project did not quite reach this stage, the process is worth examining

to better understand the eventual construction goals. First, the strong beam signal is subtracted from the weak beam signal, removing the broad absorption profiles and leaving just the Lamb Dip.

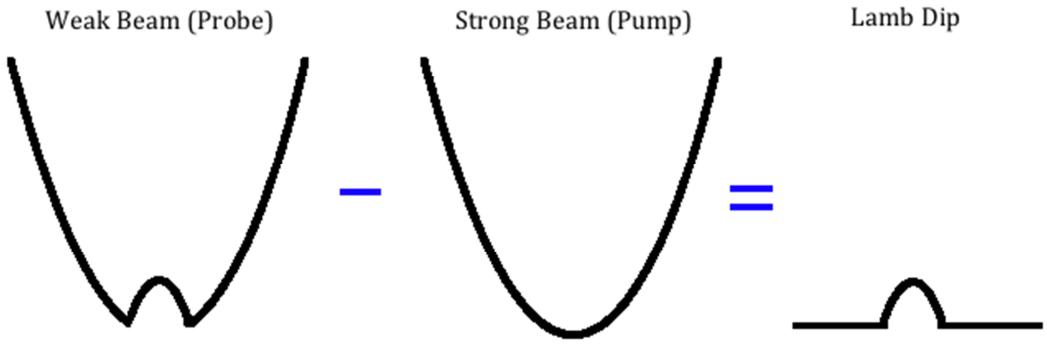

Figure 1.2: Idealized view of the clarification process of saturated absorption spectroscopy.

At this point, our variable magnetic field comes into play. Recall that we are sweeping our laser through a small range of frequencies, and the Lamb Dip pinpoints the resonance frequency. Since the Zeeman shift moves this transition frequency, a variation in the magnetic field moves our peak left or right along the frequency axis. This movement forms the basis of the electronic locking. The details, as mentioned, are beyond this thesis, but it should be noted that the precision of the locking is directly related to how rapidly we can vary the magnetic field. This comes into play in the construction phase, where we will try to create a cell with a flexible magnetic field.

1.5 Light Polarization

While the above descriptions of isotopic isolation and electronic locking are correct, it is worth examining these processes in more detail with regards to our true experimental setup. Our analysis starts with the allowed transitions for strontium shown below, with the transition we drive with our lasers highlighted:

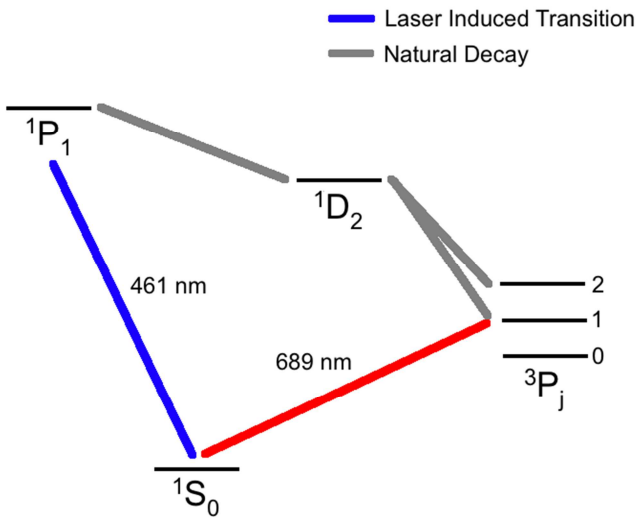

Figure 1.3: The energy levels of strontium. The red 689 nm laser is for a second stage of cooling, from the order of mK to the order of μK.

Our lasers are tuned just below the $^1S_0$ to $^1P_1$ transition, to account for Doppler shifting, at a wavelength of approximately 461 nm. The ground state $^1S_0$ is a single, non-degenerate state, meaning an applied magnetic field does not split the energy levels. The $^1P_1$ state, however, is three-fold degenerate, meaning an applied magnetic field Zeeman splits the excited state into three sublevels of spacing $\mu_B B$ (where μ_B is the Bohr magneton and B is the magnetic field): the $m = -1$ and $m = +1$ states, of lower and higher energy respectively, and the $m = 0$ state which equals the original, non-split level. This energy spacing is directly proportional to a frequency spacing, so that our photodiode will now see three rises in the broad absorption dip: one for each m value. This immediately complicates our locking scheme, as there are now essentially three Lamb Dips competing for the electronic locking. In order to focus on just one of the two shifting transitions, we turn to the polarization of our laser light.

Transitions from the ground state to each specific $^1P_1$ sublevel are induced by a certain polarization, defined with respect to the axis of the cell. Right-hand circularly (σ^-) and left-hand circularly (σ^+) polarized light drive the ground state to the $m = -1$ and $m = +1$

excited states respectively, while linearly (π) polarized light drives the original transition to the $m = 0$ state.

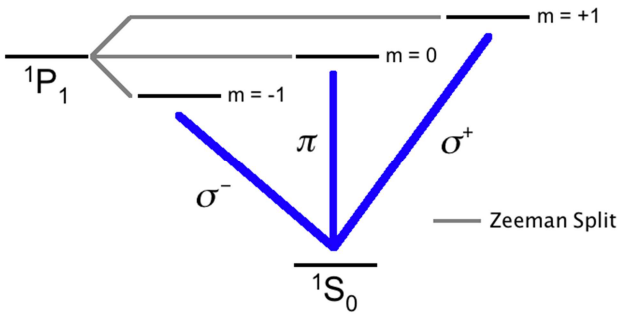

Figure 1.4: The splitting of the $^1P_1$ energy level and the light polarizations that excite each sublevel.

By selecting one of the circular polarizations (typically the left-handed σ^+) and arranging the optics so that all of the beams are of that polarization at the stage where they hit the photodiode, our absorption has only one Lamb Dip and we can use the same locking procedure as before. Knowing the relationship between applied magnetic field and increase in energy spacing of the $^1P_1$ sublevels, as well as how far the $m = 0$ sublevel is from another isotope's $^1P_1$ level, we can push the $m = +1$ sublevel up to this point, and lock on that isotope's basic excitation transition. This is a more detailed and accurate description of our experimental methods.

2. DESIGN AND CONSTRUCTION

2.1 SAS Cell

The basic design of the SAS cell derives from an earlier version currently used in one of the experiments. Any deviations from this model were meant to increase the flexibility of the Zeeman effect within the cell. Theoretically, this included doubling the magnetic field while decreasing the inductance. Given a solenoid of length l, applied current I, with N turns, and cross-sectional area A, we have the following relations for magnetic field B and inductance L (where μ_0 is the magnetic permeability constant of free space):

$$B = \mu_0 \frac{N}{l} I$$

$$L = \frac{\mu_0 N^2 A}{l}$$

Thus, to increase magnetic field, we included a larger current through the magnet wire, and to decrease the inductance, we had more coils of magnet wire and a smaller coil radius.

Before dealing with these improvements, the system had to fulfill the basic requirements for SAS: a vacuum chamber, windows for the beams to pass through, and enough heat to vaporize the strontium. The cell itself began as a foot-long stainless steel tube, held up by two stands machined out of aluminum to bring it to the level of the laser on the optics table. Special flanges were welded to each end in order to attach vacuum-tight windows specifically designed to transmit as much of the beams as possible. Another smaller and shorter tube was welded perpendicular to the original tube, as near the end as possible without blocking the stand. This tube served as an attachment to a vacuum pump, which was used at first to leak test the welds and eventually to bring the sample near vacuum conditions (schematics of all of these components can be found in the Appendix).

Figure 2.1: Bare cell, showing the tube with attached flanges. The protrusion on the left is the vacuum connection without its valve, and the windows are currently not attached to the ends.

With the basic design complete, attention was shifted to heating capability and increased magnetic flexibility. The vaporization temperature of strontium is extremely high – on the order of 1400 degrees Celsius – but we do not need to vaporize the entire sample. In fact, temperatures around 400 – 500 degrees Celsius are sufficient to sublimate enough strontium vapor into the cell. While that's much cooler than the boiling point, it necessitates active heating along with a good deal of insulation on the cell. Active heating was achieved through tightly-wound heating cable brazed to most of the exterior of the main tube. Thermocouple wire was brazed to the heating cable for future temperature monitoring and for design testing – we now added insulation layer by layer and tested the heating capability of the cell at each subsequent iteration until we reached an appropriate amount beyond the desired temperature.

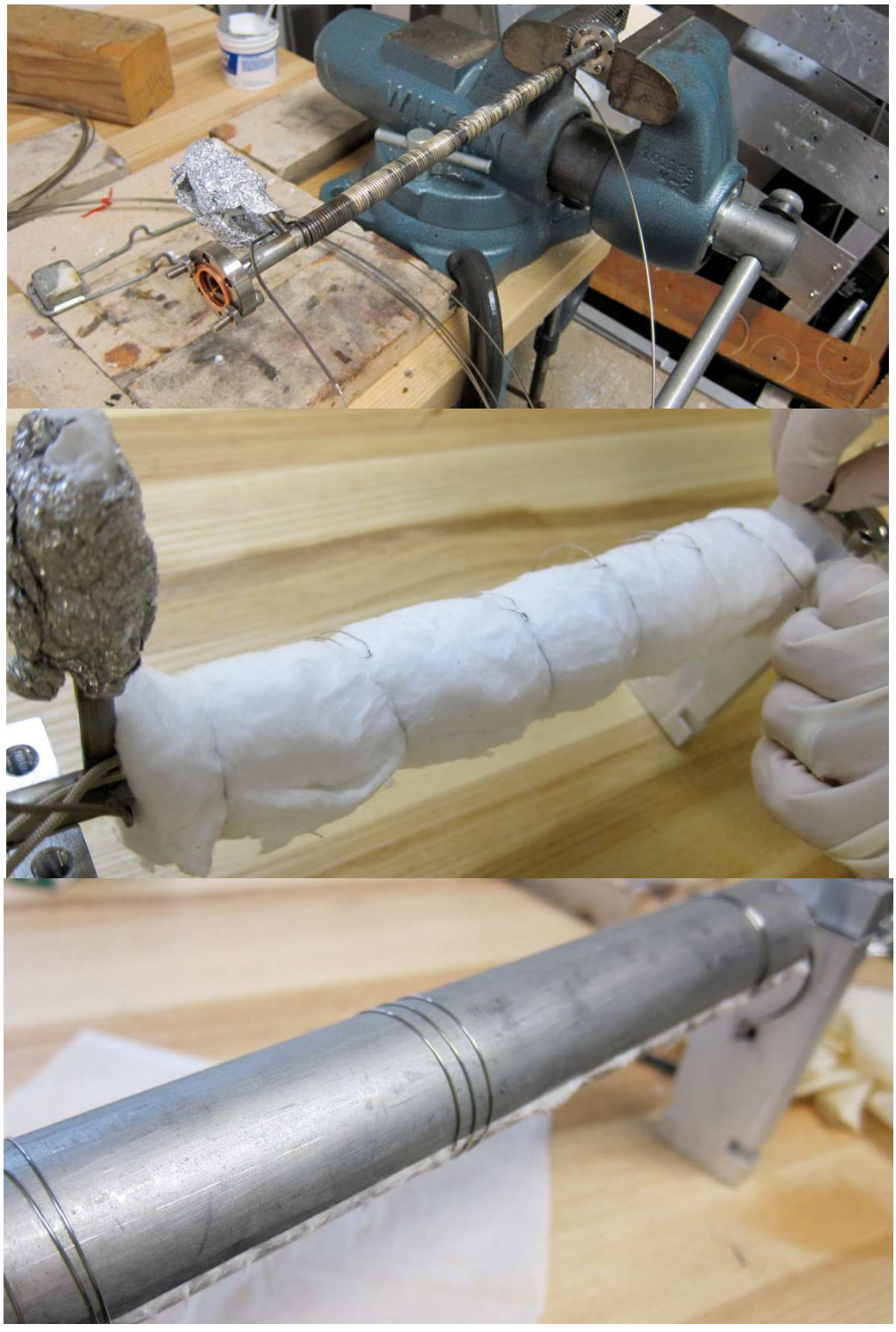

Figure 2.2: In sequential order: vapor cell wrapped in heating cable, already brazed to surface; vapor cell wrapped in a layer of fiberglass insulation above the heating cable; stainless steel semi-tubes used to compress insulation and onto which the magnet wire was wrapped.

So far, two minor problems have arisen – firstly, our magnet wire cannot withstand very high temperatures, meaning it has to be separated from the cell by a few layers of insulation. Given our desire to decrease the radius of the magnetic coils as much as possible, we measure the surface temperature at each insulating level until we deem it cool enough to wrap our magnet wire. Secondly, the stands and vacuum connection shortened the length we could insulate, and therefore the length we could wrap. The shorter the wrapping length, the less turns of coil, and the weaker the field. Thankfully, we still had 22.86 cm to wrap, longer than the old cell's 21 cm.

First, everything was enclosed in sheets of fiberglass insulation, which in turn were compressed by two 0.625" radius stainless steel semi-tubes. The temperature on these semi-tubes was deemed cool enough to wrap our magnet wire, so next came three layers of tightly-wound magnet wire. To offset the effect of forthcoming insulation increasing the temperature past the magnet wire's capacity and simply to prevent shorting, the first two layers of magnet wire were sleeved in fiberglass insulation. The final layer was wound bare in the grooves of the second layer, again preventing shorting.

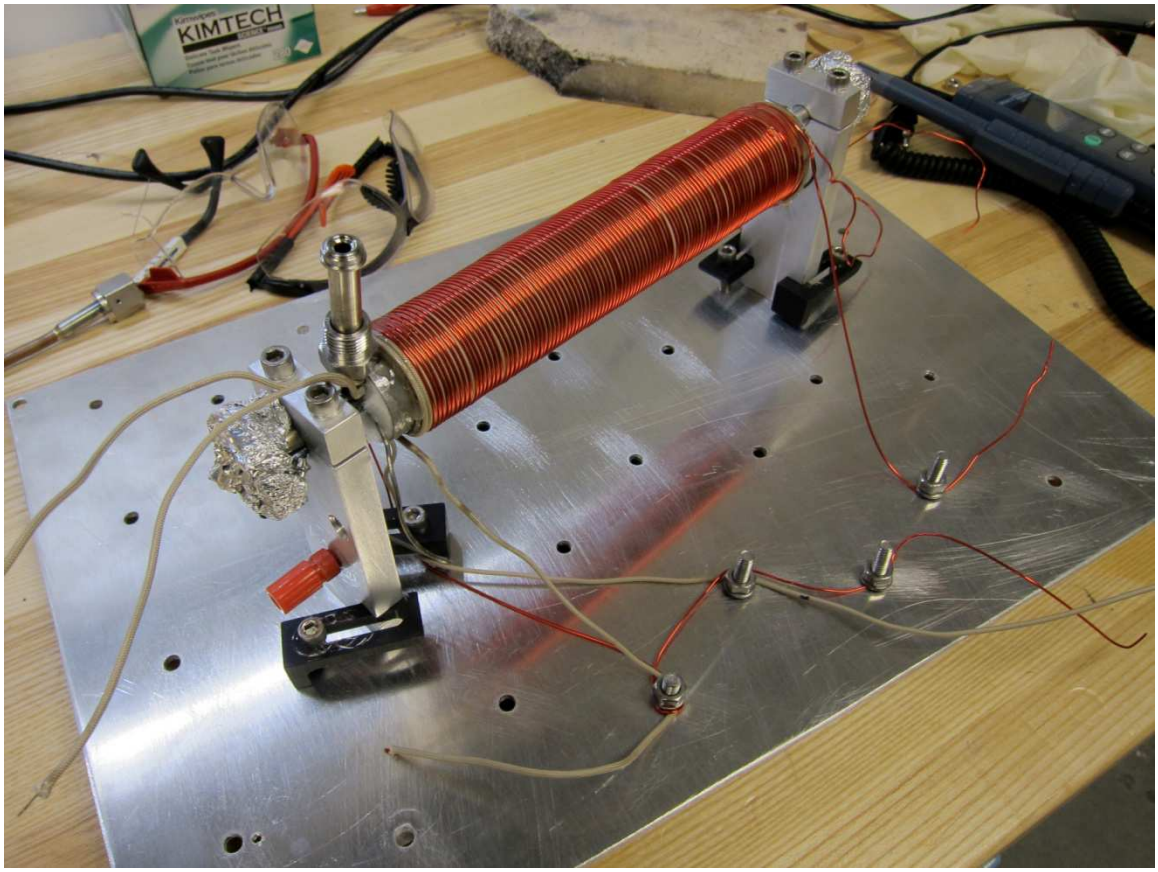

Figure 2.3: Vapor cell on stands, with two layers of magnet wire in tan, insulating fiberglass sleeving and a final layer of the bare red wire. The insulated pair of wires coming out on the left are the thermocouple.

A thick layer of epoxy baked the magnet wire into place, in turn covered by more sheeted fiberglass insulation. A few layers of tin foil brought the cell up to the desired temperature range, finishing off the insulation of the tube.

The ends of the heating cable were soldered to binding posts in the stands, allowing direct connection to the electronics for temperature control. Each layer of magnet wire had to attach to the opposite end of the next layer – this was done beyond the insulation, so the wires come outside the cell, labeled as to which belongs to which layer. The beginning of the first layer and the end of the third layer are connected to a BNC post in one of the stands, allowing direct connection to the electronics for field control. The small grooves in the bottom of the stands help secure the cell to the optics table, as demonstrated above.

2.2 Complimentary Electronics

Electronics design was also based on the flexibility of the Zeeman effect within the cell. Namely, our increased magnetic field relied on a high current through the magnet wire, while rapid variation of the magnetic field (for locking purposes) relied on low impedance.

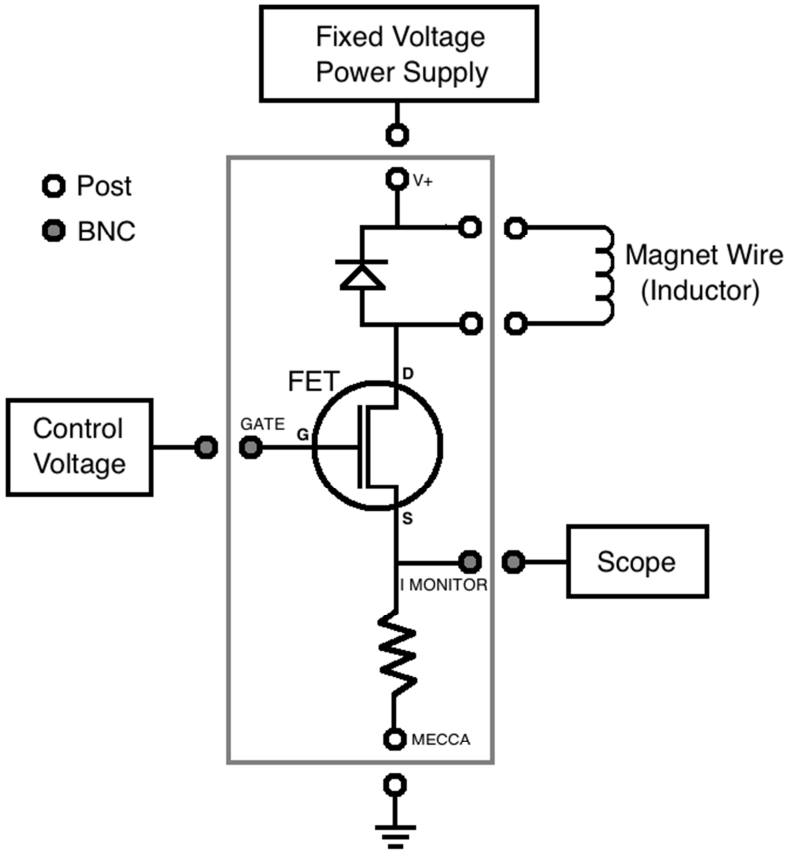

Figure 2.4: Basic circuit used throughout this thesis. All BNCs, power supplies, and the scope were grounded to MECCA. We use a 13.8 V TENMA Regulated DC Power Supply, Model 72-8142, as our fixed voltage power supply. Eventually, a feedback circuit will be added to perform the actual electronic locking.

In the circuit, our resistor acts as a simple current monitor – voltage across the resistor is converted to current input into the magnet wire. By varying the gate voltage of the FET, we can vary the current from the fixed voltage power supply, essentially giving us a variable resistor. The circuit seen above was tested for DC response, and gave the following results:

V_{GS} (V)	$V_{monitor}$ (V)	I (A)
5.1	1	10
4.9	0.9	9
4.7	0.8	8
4.6	0.7	7
4.4	0.6	6
4.3	0.5	5
4.2	0.4	4
4.0	0.3	3
3.9	0.2	2
3.7	0.1	1
3.5	0.05	.5
3.0	0	0
2.0	0	0
1.0	0	0
0	0	0

Table 2.1: For our DC response test, we connected I MONITOR to CH1 of the Scope and the Control Voltage branched to both the GATE and CH2 of the Scope. A function generator (not shown) triggered the Scope. V_{GS} is the voltage from the gate to source, or in the diagram, GATE to MECCA. $V_{monitor}$ is the voltage across the magnet wire, or I MONITOR to MECCA. With the resistor being 0.1 Ω we can easily convert this voltage to current I.

The eventual goal would be better control over the current in the magnet wire, specifically so that the current out is linearly proportional to a control voltage. This will be accomplished by a feedback circuit designed and implemented by Xizheng Ma, which would build off of the schematic above.

For a solenoid such as our cell (with N turns), Faraday's law of induction states that for change in magnetic flux over time $\frac{d\Phi_B}{dt}$, the back emf ε generated is:

$$\varepsilon = -N\frac{d\Phi_B}{dt}$$

Thus, our desire for rapid variation of the magnetic field leads to high back emf, essentially slowing down that rapid variation by making it difficult to quickly change the current. With the FET and fixed voltage power supply, we found we could modulate the current at several kHz, which is satisfactory for our application.

2.3 Temperature Controller

Once the strontium is vaporous, the higher the temperature in the cell, the wider the absorption spectrum. In essence, as temperature rises, average atomic velocity rises, and the distribution of parallel velocities to the laser widens, which in turn widens the absorption. Keeping in mind a general desire for clarity in our data, it is therefore important that temperature within the cell is relatively stable so that our absorption is narrower. Tweaking the voltage across the heating cable gives us a steady value for temperature inside the cell, with no noticeable fluctuation. A problem arises, however, when the magnet wire runs. Due to its high current and three layers, the wiring that drives our magnetic field appreciably heats the cell. Furthermore, the field is, by design, variable, meaning the heating contribution of the magnet wire is variable. This presents a need for temperature stabilization, which comes in the form of a temperature controller.

The main component of the controller is a commercially purchased Watlow EZ-ZONE PM Integrated Controller. This component has inputs for the thermocouple from the cell as well as connections to hook into the heating cable circuit. Given a desired temperature to maintain, the Integrated Controller decides how much power flows from the DC power supply and into the heating cable, based on the reading from the thermocouple wire. In the event of a malfunction leading to continuous of the cell, a solid-state relay has also been wired into the heating cable circuit, which can be programmed to stop all current at a given maximum temperature as read by the thermocouple. As an added bonus, an on-off switch is also wired into the heating circuit, giving the option of turning off the heating cable but still reading the temperature from the Integrated Controller. Schematics of the Temperature Controller design and connections can be found in the Appendix.

3. APPLICATION

3.1 Basic Spectroscopy

Before running full saturated absorption spectroscopy, we ran a lone probe beam through the cell and onto the photodiode, without the counter-propagating pump beam that arises in SAS. As explained in the section on SAS, this gave us a Doppler-broadened absorption profile, without the Lamb Dip that comes from the beam-crossing. Monitoring the voltage drop through the photodiode, we could determine the ideal voltage to run across the heating cable to get the desired temperature and therefore the desired absorption profile.

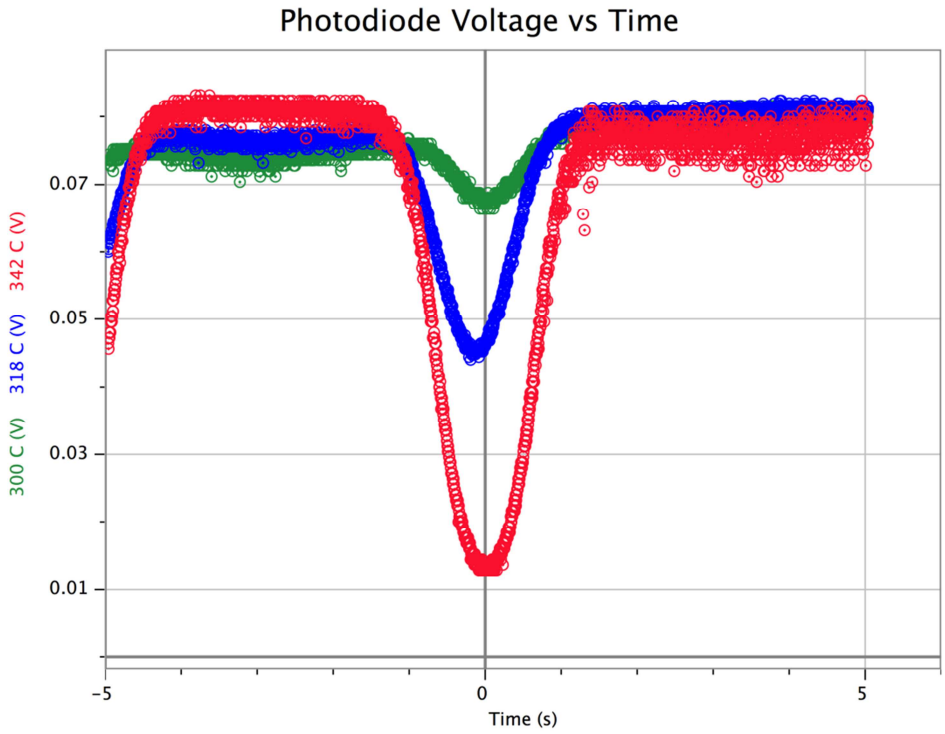

Figure 3.1: Raw data from the oscilloscope of our basic spectroscopy. The blue corresponds to no absorption, green to low absorption, orange to over-saturation, and red to nearly 100% absorption.

Taking the percentage absorption to correspond to the depth of the profile, we used outputs such as those in the figure above to determine what percentage absorption

corresponded to what temperature reading off of the thermocouple wire brazed to the heating cable. As we will see, this temperature is not necessarily the temperature of the strontium vapor, so for clarification, we will use the terms cell temperature and vapor temperature. With this in mind, we can quickly plot absorption versus cell temperature. In addition, given the voltage reading for the heating cable on our DC power supply and knowing the resistance through the cables, we can also plot absorption versus applied current, as well as cell temperature versus applied current.

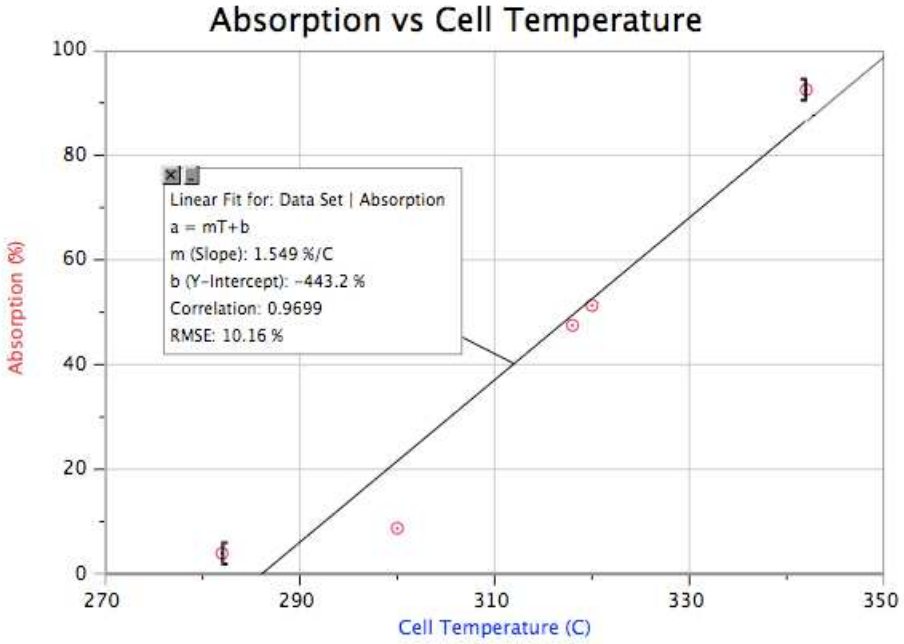

Figure 3.2: Graph showing the positive correlation between temperature and absorption percentage, measured directly as the voltage drop across the photo-diode.

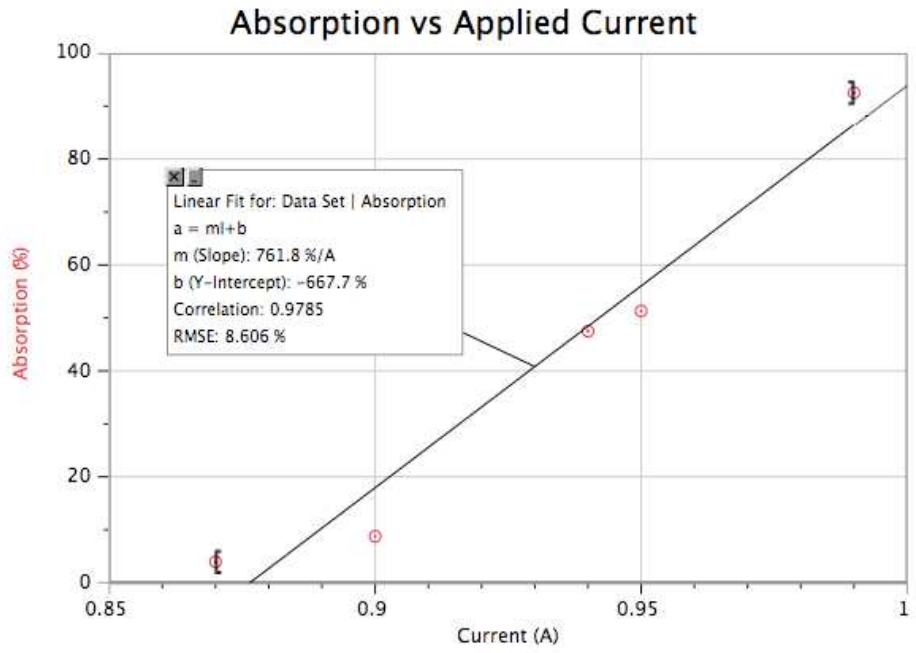

Figure 3.3: Similar graph showing the positive correlation between applied current and absorption percentage.

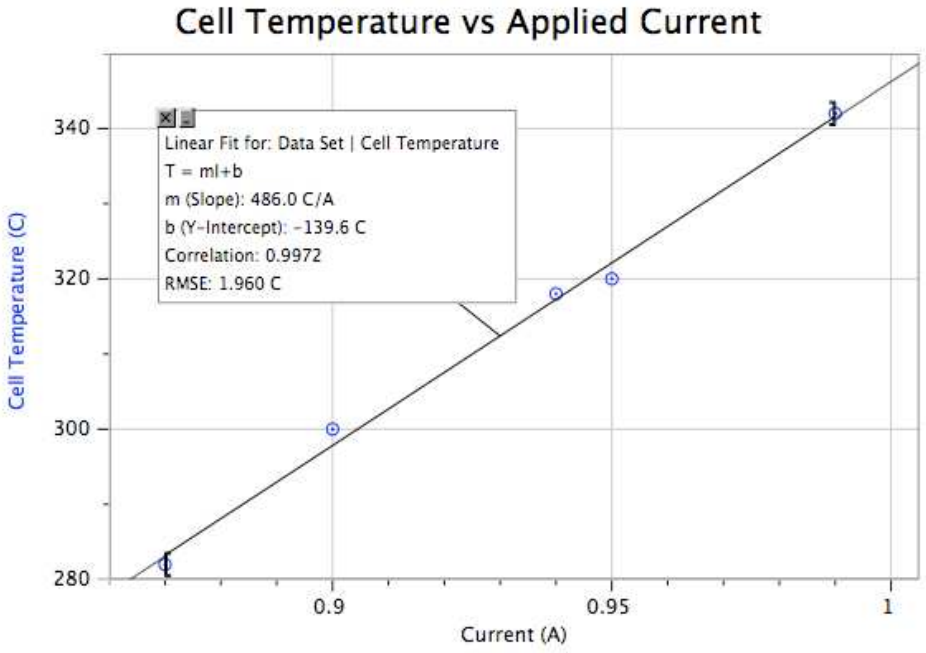

Figure 3.4: Relationship between temperature reading off the heating cable and the current applied through the heating cable.

Given this data, Beer's law gives us a formula with which we can find the strontium vapor density n_{Sr} [2]:

$$n_{Sr} = -\frac{1}{\sigma l}\ln\left(\frac{I}{I_0}\right)$$

Here, l is the cell length, and I_0 is the intensity of the light entering the sample while I is the intensity of the light exiting the sample and hitting the photodiode, so that $\frac{I}{I_0}$ corresponds to the absorption percentage. While these values are known, the absorption cross-section σ for strontium vapor is a significantly more complex problem, due to its dependence on a number of factors.

For an isolated strontium atom at rest in the ground state, the absorption cross-section near resonance with the $^1S_0$ to $^1P_1$ transition (at λ = 461 nm) is given by the Lorentzian [3]:

$$\sigma(f) = \frac{\sigma_0}{1+\left[\frac{2(f-f_0)}{\gamma}\right]^2}$$

Here we have the cross-section in terms of frequency, where $\sigma_0 = \frac{3\lambda^2}{2\pi}$ is the peak absorption cross-section for a two-level atom such as our own [4], γ = 30.5 MHz is the natural transition linewidth for $^1S_0$ to $^1P_1$, and $f_0 = \frac{c}{\lambda}$ is the resonant frequency (for speed of light c).

As explained previously, our sample does not have these ideal conditions because the atoms have thermal motion. For an atom moving with velocity v, the resonance frequency shifts by $\frac{kv}{2\pi} = \frac{v}{\lambda}$ where $k = \frac{2\pi}{\lambda}$ is the wavevector of the light. With this shift, the absorption cross-section becomes:

$$\sigma(f,v)=\frac{\sigma_0}{1+\left[\frac{2[f-(f_0+v/\lambda)]}{\gamma}\right]^2}$$

This equation only considers velocity in the direction of the wavevector because only the component of each velocity parallel to the laser direction affects the absorption.

We now have to determine the effect of the entire set of possible velocities for the atoms. For a typical thermal sample of atoms of mass m at temperature T, the normalized distribution of the velocities is a Maxwell-Boltzmann distribution (where k_B is the Boltzmann constant):

$$g(v)=\sqrt{\frac{m}{2\pi k_B T}}\exp\left[-\frac{mv^2}{2k_B T}\right]$$

Convoluting this Gaussian distribution and the Lorentzian expression, we have the average absorption cross-section as a function of laser frequency (known as a Voigt profile):

$$\langle\sigma(f)\rangle=\int_{-\infty}^{\infty}g(v)\sigma(f,v)dv$$

We can simplify our analysis by noting that the broadening due to Doppler shifts $\delta f=\frac{1}{\lambda}\sqrt{\frac{k_B T}{m}}$ is much larger than the natural linewidth. Then we can approximate our Lorentzian as a delta function with the relation:

$$\lim_{\gamma\to 0}\frac{2\pi}{\gamma}\left(1+\frac{4x^2}{\gamma^2}\right)^{-1}=\delta(x)$$

Then our Lorentzian becomes:

$$\sigma(f,v)=\frac{\sigma_0\gamma}{2\pi}\delta[f-(f_0+v/\lambda)]$$

With this modification, and using the delta function relations $\delta(-x)=\delta(x)$ and $\delta(\alpha x)=\frac{\delta(x)}{|\alpha|}$ for constant α, we can now write our convolution as:

$$\langle \sigma(f) \rangle = \frac{\sigma_0 \gamma}{2\pi} \int_{-\infty}^{\infty} g(v) \lambda \delta[v - \lambda(f - f_0)] dv$$

Finally, since the delta function has the property $\int_{-\infty}^{\infty} g(v)\delta(v - x)dv = g(x)$, we have:

$$\langle \sigma(f) \rangle = \frac{\sigma_0 \gamma \lambda}{2\pi} \sqrt{\frac{m}{2\pi k_B T}} \exp\left[-\frac{m\lambda^2 (f - f_0)^2}{2k_B T} \right]$$

It is important to note that the temperature T came from the expression for a Maxwell-Boltzmann distribution of atoms, meaning it is the temperature of the strontium vapor itself, which is not quite the same as the cell temperature measured off of the thermocouple. Now, if we assume that the vapor temperature and the vapor density are constant throughout the heated length l, we can fit the experimental absorption spectrum using Beer's law:

$$\frac{I(f)}{I_0} = \exp\left[-n_{Sr} \langle \sigma(f) \rangle l \right]$$

Here we have edited our previous formula to account for the true cross-section value being an average and noting the frequency dependence of the outgoing light intensity. In order to truly match the formula to our raw data, we need to fit to an expression of the following form:

$$I(f) = (I_0 + \Delta I f) \exp\left[-n_{Sr} \langle \sigma(f) \rangle l \right]$$

The $(I_0 + \Delta I f)$ term accounts for the vertical offset I_0 (since the incoming intensity gives a high value rather than zero) and the intensity slope ΔI caused by a slight change in laser power as we sweep through our frequency range.

Since our original output is actually outgoing light intensity versus time, we also need to convert the horizontal axis to frequency. This simple process is explained in the Appendix. With this taken care of, we now fit our data to the function above in order to extract vapor density, vapor temperature, vertical offset, and intensity slope. By the nature

of our time to frequency axis conversion, we also extract a value for “resonance frequency” which in this case is really deviation from resonance.

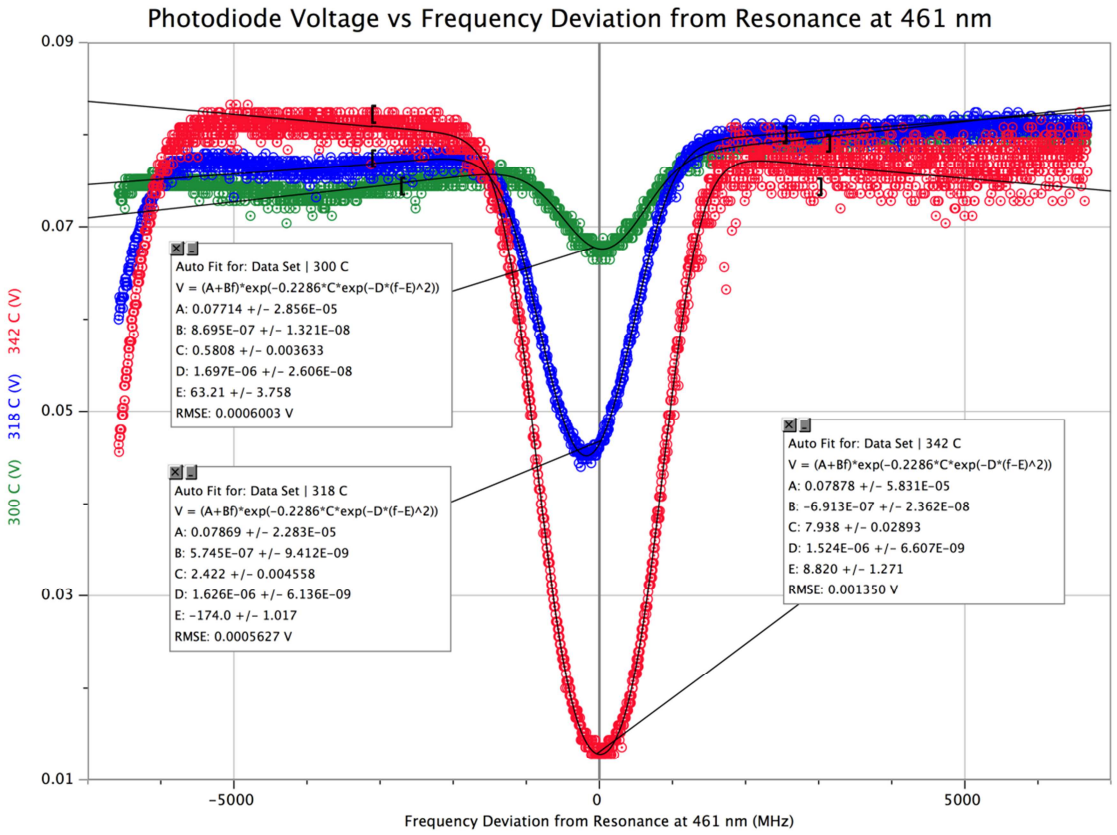

Figure 3.5: Example of three fits of our raw spectroscopy data. Green, blue, and red correspond to cell temperatures of 300 C, 318 C, and 342 C respectively. Small brackets show the range of the fit, which did not include the anomaly on the far left.

There is a short summary of parameter extraction in the Appendix, explaining how the above values translate into the desired parameters. These fits yield plots of vapor temperature versus cell temperature and vapor density versus cell temperature.

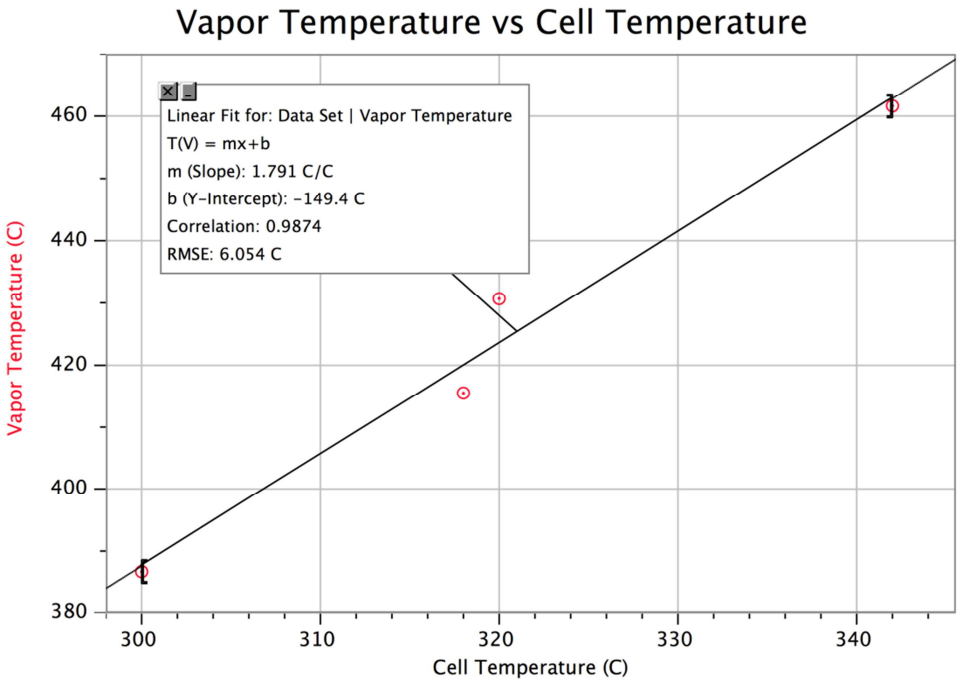

Figure 3.6: Relationship between vapor temperature and cell temperature, in degrees Celsius.

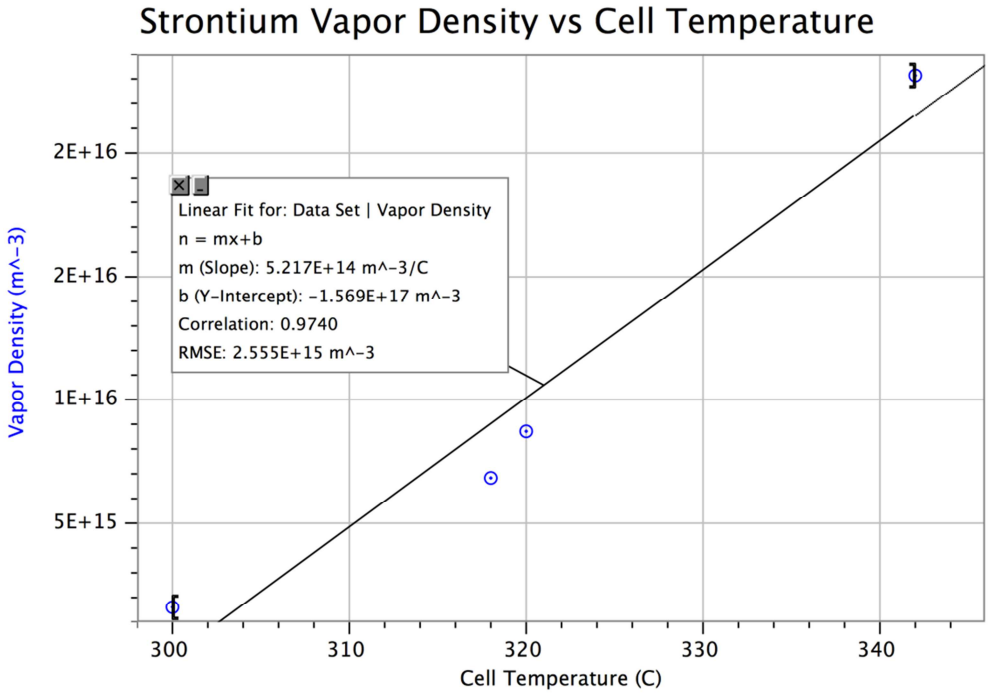

Figure 3.7: Relationship between strontium vapor density and cell temperature.

3.2 Saturated Absorption Spectroscopy

Having encountered no problems with the regular spectroscopy, we moved on to full saturated absorption spectroscopy. With the counter-propagating beam running, our goal was to see our Lamb Dip on the photodiode voltage reading of the oscilloscope. With no current running through our magnet wire, and therefore no Zeeman splitting, we fit the Lamb Dip to a Lorentzian:

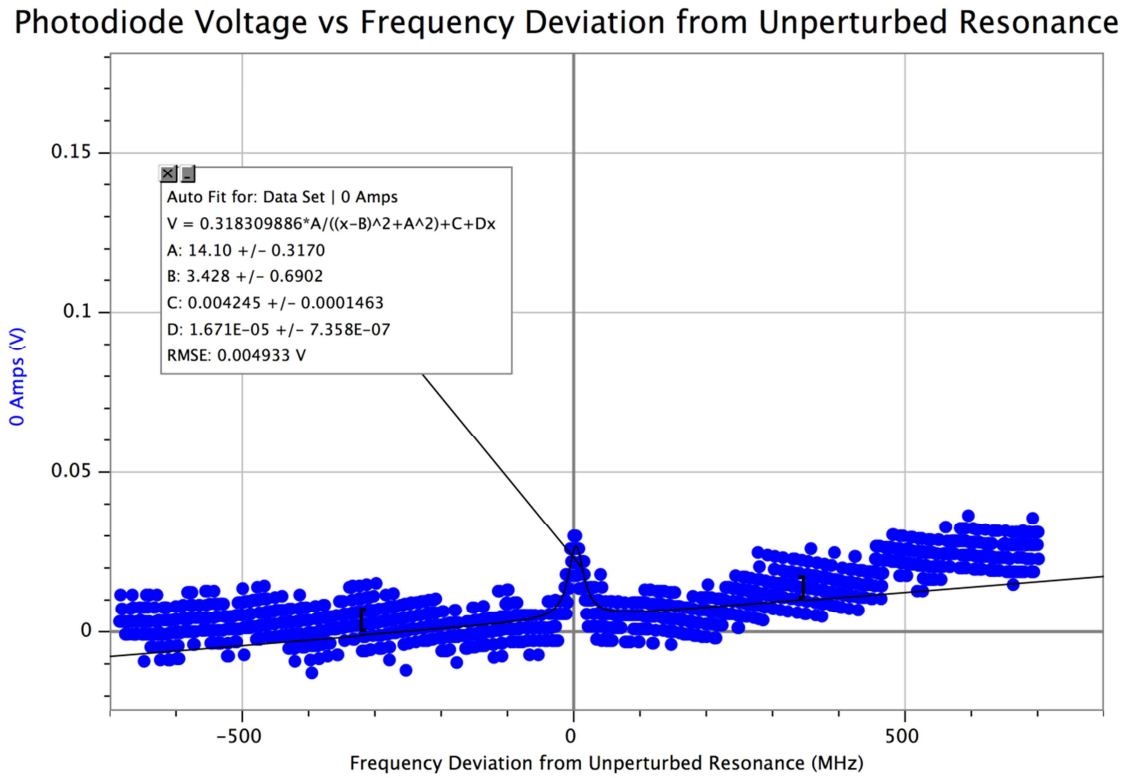

Figure 3.8: Lorentzian fit for the unperturbed spectrum. Note that the broad dip has been flattened, as shown in Figure 1.2. From this we can extract the full width at half maximum, as below.

As with all the oscilloscope outputs, our plots began with photodiode voltage versus time. Our fits are based on frequency however, so the horizontal axis had to be converted. The methodology for this simple process is outlined in the Appendix. With this fit, we extract the full width at half maximum, which equals the natural linewidth of the transition. The fit above gives $\gamma = 28.20$ MHz, within a reasonable range of the known $\gamma = 30.5$ MHz.

3.3 Zeeman Splitting

With SAS working as desired, it remained to test the ability of the variable magnetic field to split the transition. With the cell running as before, we drove current through the magnet wire at various levels. Ideally, our design will follow the aforementioned relation:

$$B = \mu_0 \frac{N}{l} I$$

Given our cell length of 22.86 cm, and 104 turns per layer (312 turns total), we have the following relationship between applied current and magnetic field:

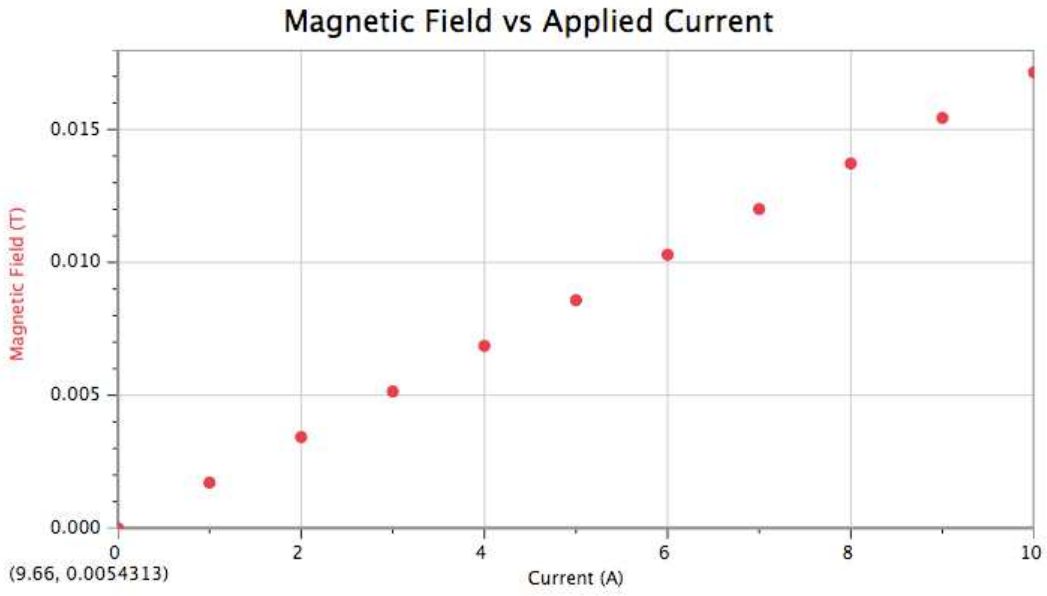

Figure 3.9: Graph of direct relationship between applied current and magnetic field in our cell, with slope 0.001715 T/A.

Recall that the change in transition frequency for an applied magnetic field is proportional to the energy spacing. For frequency shift f, magnetic quantum number m, and with the previously mentioned Bohr magneton μ_B, the actual relation is (where h is the Planck constant):

$$f = m \frac{\mu_B B}{h}$$

With this, we can plot frequency shift of the transition versus applied current:

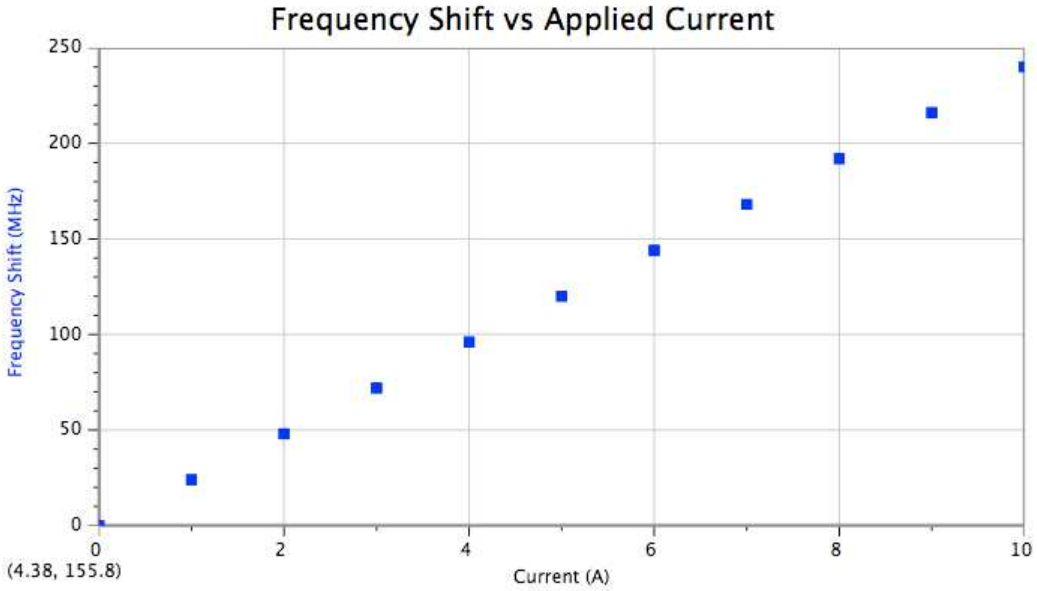

Figure 3.10: Graph showing the change in transition frequency for a given applied current, with slope 24 MHz/A.

With our apparatus, we took spectra for the magnet wire at 0 amps (shown in Figure 3.8), 2.5 amps, 7.5 amps, and 10 amps. As the applied current increased, we saw the Lamb Dips of the $m = -1$ and $m = +1$ sublevels moving left and right from the center Lamb Dip. To demonstrate this shift visually, we took the same frequency range of the four different spectra and separated them vertically by an amount proportional to the applied current (so that 10 amps was 3 times higher than 2.5 amps, etc). One can then find a linear fit through both sets of Lamb Dips on the left and on the right to show the Zeeman shift.

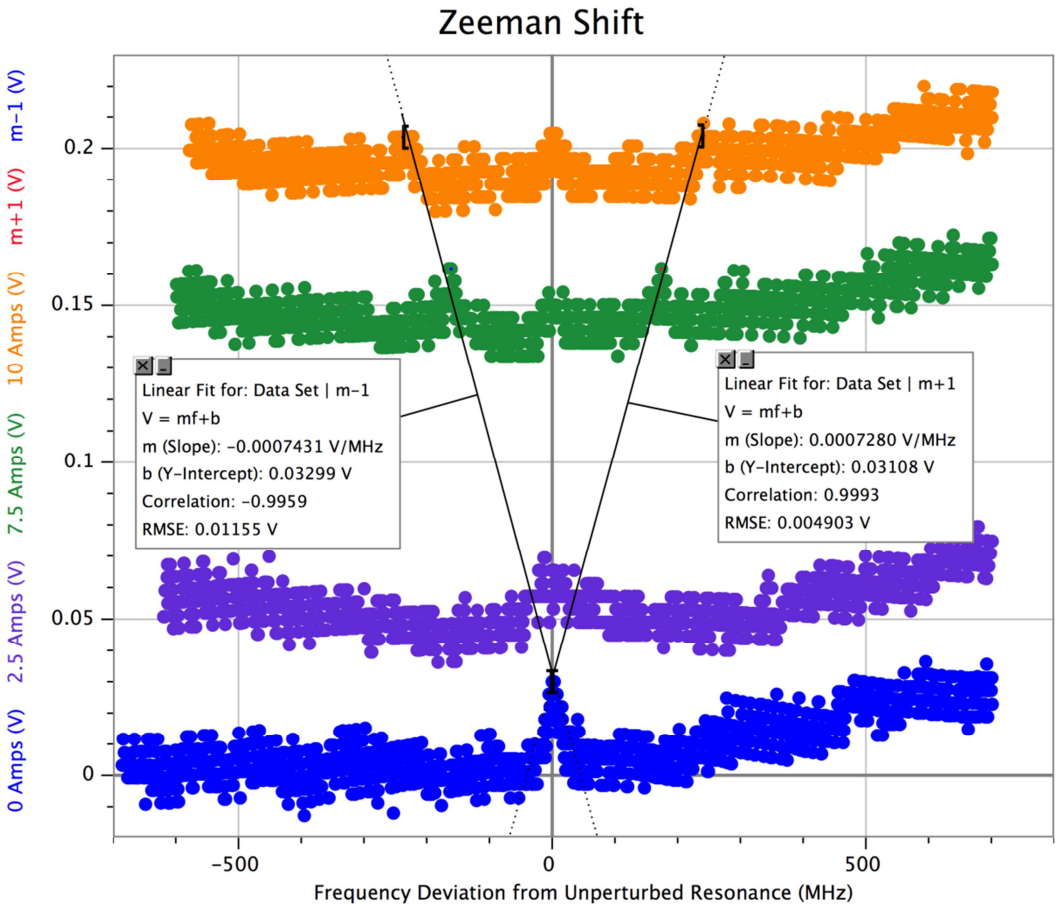

Figure 3.11: Here we have four spectra at various applied currents, showing the Zeeman shift. The spectra have been vertically separated by an amount proportional to the applied current, so that we can fit lines through the peaks to demonstrate the Zeeman shift visually. In other words, the actual data would all sit near zero voltage but this way we see the m=+1 and m=-1 peaks moving right and left respectively.

4. CONCLUSION

In conclusion, the desired development of a saturated absorption spectroscopy cell to accurately tune the laser was a success – the Lamb Dip was clearly visible, and the observed natural linewidth was reasonably within agreement of the known value. In addition, the variable magnetic field of the cell, coupled with the complimentary electronics, met or exceeded design expectations of flexibility and strength. It was successfully implemented to observe the Zeeman splitting of the levels, and it remains to complete the locking elements of the circuit to render the entire apparatus fully functional.

5. REFERENCES

[1] Newport. *FM Spectroscopy With Tunable Diode Lasers: New Focus Application Note 7*. Retrieved from http://www.newport.com/New-Focus-Application-Note-7-FM-Spectroscopy-With/979109/1033/content.aspx

[2] Vogel, K.R. (1999). *Laser Cooling on a Narrow Atomic Transition and Measurement of the Two-Body Cold Collision Loss Rate in a Strontium Magneto-Optical Trap* (Doctoral dissertation). Rice University, Houston, TX.

[3] Demtroder, W. (2008). *Laser Spectroscopy* (Vols. 1-2). (4th Ed.). Berlin, Germany: Springer-Verlag.

[4] Foot, C.J. (2005). *Atomic Physics* (pp. 141-142). New York, NY: Oxford University Press.

6. APPENDIX

6.1 Parts & Schematics

SAS Cell schematics:

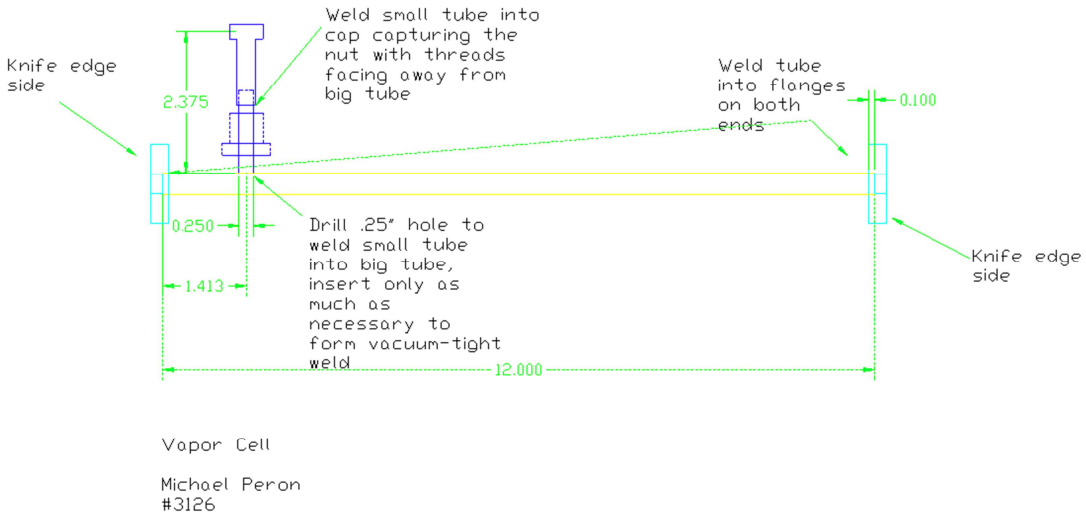

Figure 6.1: Machine shop drawing of the basic cell. Light blue flanges are shown, along with the dark blue vacuum connection.

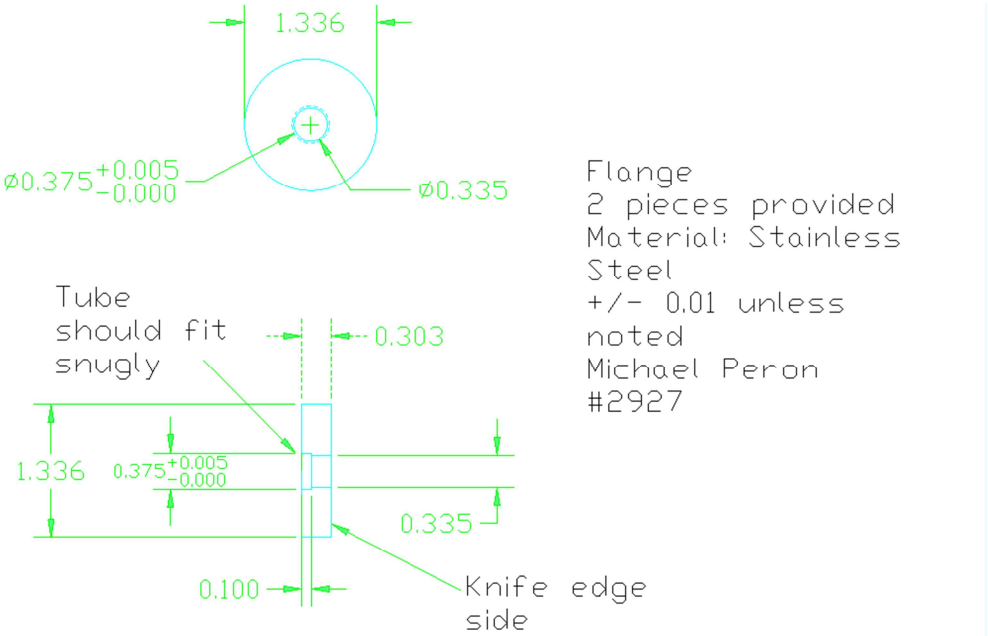

Figure 6.2: Machine shop drawing of our flanges.

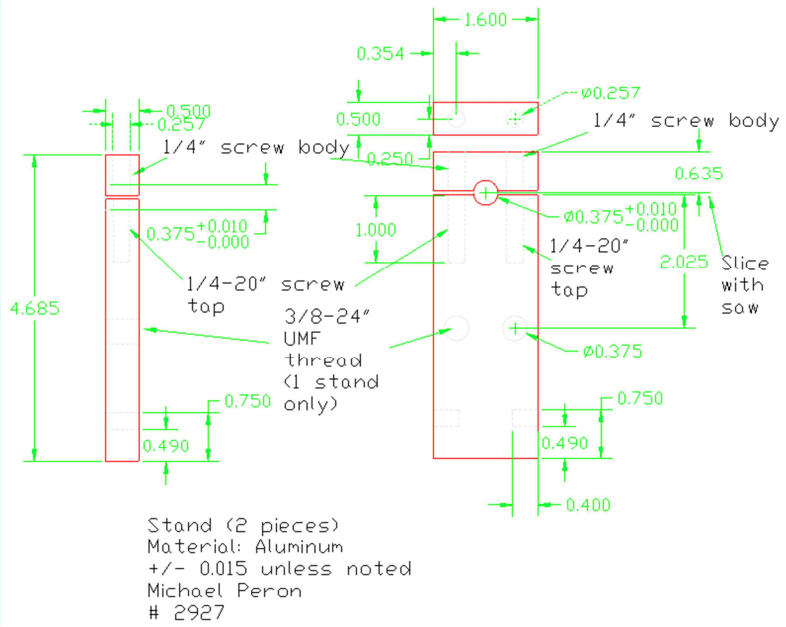

Figure 6.3: Machine shop drawing of the stands.

SAS Cell components:

- Stainless Steel 304L Seamless Round Tubing (72” long, 0.375” outer diameter, 0.02” thick wall)
- Stainless Steel Round Tubing (9” long, 1.25” outer diameter)
- Aluminum stands, machined at the machine shop
- 40’ of 1.6 ohm/ft heating wire from ARi Industries (Part No 1HN063B-1.6)
- 2x 100’ spools of fiberglass insulation wire from SPC Technology
- 150’ of Thermal Class 155 NEMA MW 80-C Red Magnet Wire from Wiretron
- Sheets of fiberglass insulation
- Emerson & Cuming STYCAST 2762 Epoxy mixed with Catalyst 14 at a ratio of 100 to 8, eventually using about 50 g epoxy to 4 g catalyst to cover the entire cell
- Regular tin foil
- 4’ of thermocouple wire

Electronics components:

- IXYS IXFN340N07 MOSFET
- Ohmite 850FR10 0.1 Ω resistor, 50 W rated
- Note: All connecting wires are rated for a high current, as up to 10 A will run through the magnet wire
- Note: The MOSFET and resistor were placed on a heat sink
- Note: The electronics may be modified for the inclusion of the eventual feedback circuit

Temperature Controller schematics:

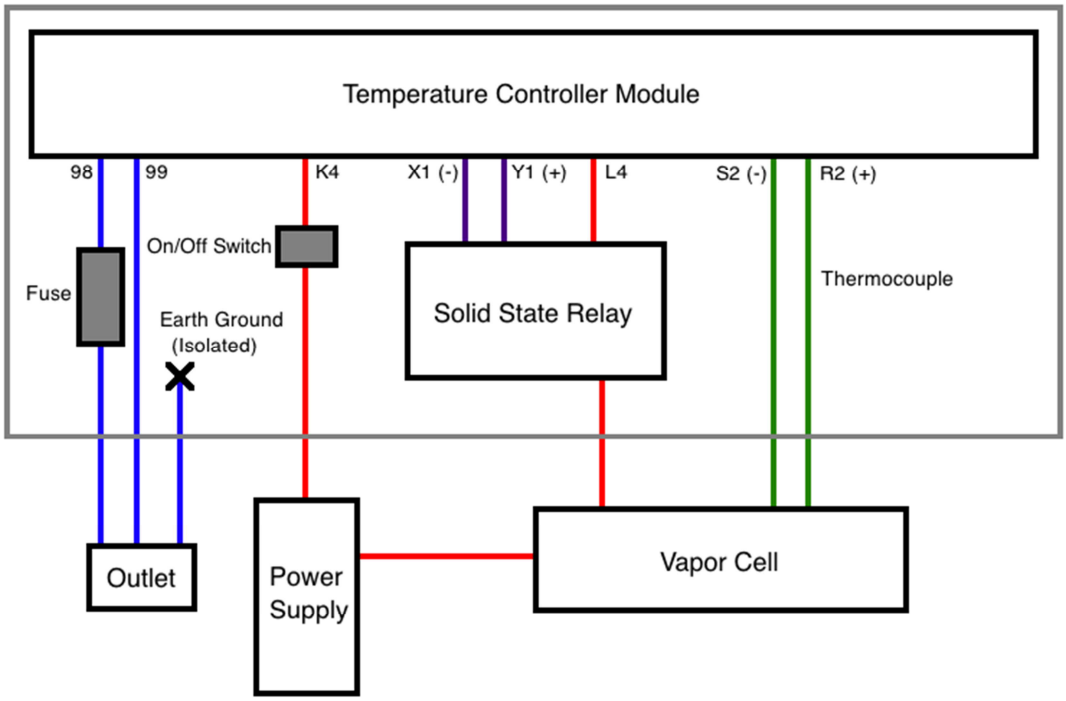

Figure 6.4: Diagram of the connection of the temperature controller to the entire experiment. Labels indicate where various wires connect to the controller module itself. Colors indicate different circuits/wires.

Temperature Controller components:

- Watlow EZ-ZONE PM 6C1CA-ALAJAAA Temperature Controller module
- Watlow Controls Solid State Relay SSR-240-10A-DC1
- Three prong on/off switch

- Note: The SSR was placed on a heat sink

6.2 AC Response Test

Here is the data for the AC response test:

$V_{GS, avg}$	ΔV_{GS} (mV)	f (Hz)	$\Delta V_{monitor}$ (mV)	Comments
Voltmeter: 3.70 V Control Supply: 3.8 V Fixed Supply: 3 A (Expect 1A)	59	100	30	no phase shift
	59	300	30	
	60	1000	29	
	69	3000	34	
	76	5000	37	
	--	~7000	--	distortion begins, still no phase shift
Voltmeter: 3.90 V Control Supply: 4.0 V Fixed Supply: 5 A (Expect 3A)	60	100	38	no phase shift
	60	300	38	
	60	1000	38	
	73	3000	40	
	86	4000	55	
	97	5000	59	
	72	6000	42	
	56	7000	36	
	48	8000	30	
Voltmeter: 4.17 V Control Supply: 4.3 V Fixed Supply: 7.5 A (Expect 5A)	57	100	36	no phase shift
	58	300	39	
	60	1000	40	
	80	3000	55	
	82	4000	55	
	68	5000	45	
	50	6000	34	
	36	7000	23	
	19	8000	16	

Table 6.1: For our AC response test, we built an RC circuit to create the small wiggles desired. This RC circuit had a DC input, connected to the Control Voltage, and an AC input, connected to the function generator. It had an output straight to Scope CH1 and a monitor output connected to I MONITOR and a Voltmeter, for more accurate voltage readings. The function generator also connected to Scope CH2. Above we see the voltage reading on the Voltmeter, the Control Voltage, and the Fixed Voltage Power Supply.

6.3 Axis Conversions

There were two axis conversion schemes in this thesis, one for the basic spectroscopy, and another for the Zeeman shift spectroscopy. Both involved a conversion of a time axis into a frequency axis, but due to the data available, each was handled differently.

For the basic spectroscopy, we have a ramping signal running at the same time as we take the absorption data. This signal gives a steadily increasing intensity reading as we scan the laser across a range of frequencies. While it would seem logical to scan around the resonance frequency at 461 nm, lasers in that range tend to be exceedingly costly. A simpler solution is to run a much cheaper infrared laser at double the wavelength (so half the desired frequency range), around 922 nm, and use non-linear optics techniques beyond the scope of this thesis to double the frequency before the laser reaches the cell. In the analysis presented in this thesis, for example, the scanning range is 921.716 nm to 921.729 nm. Converting those to frequency, we get a frequency range of the ramp signal from low point to high point. Using the oscilloscope data, we can find the time values for the low point and high point, and so we have a change in time corresponding to a change in frequency value, allowing us to convert the axis.

For the Zeeman shift, we find the time value for the 10 amp m=0 and m=+1 or m=-1 peak, and subtract those time values to get the time shift for a 10 amp increase in applied current. Our data tells us we also have a 24 MHz/A change in frequency over applied current, which means for the time difference found, there is a 240 MHz change in frequency, allowing us to convert the axis.

6.4 Parameter Extraction

In the basic spectroscopy, our data was expected to fit the following equation:

$$I(f) = (I_0 + \Delta I f)\exp\left[-n_{Sr} l\left\{\frac{\sigma_0 \gamma \lambda}{2\pi}\sqrt{\frac{m}{2\pi k_B T}}\exp\left[-\frac{m\lambda^2 (f - f_0)^2}{2k_B T}\right]\right\}\right]$$

Here we have inserted the average cross-section equation into the intensity equation to show the full expression. In LoggerPro, the graphs were fit to the following equation, where the length of 0.2286 m was already included:

$$I(f) = (A + B * f)\exp(-0.2286 * C * \exp(-D * (f - E)^2))$$

Therefore, we have the following relations:

$$A = I_0$$

$$B = \Delta I$$

$$C = n_{Sr} \frac{\sigma_0 \gamma \lambda}{2\pi} \sqrt{\frac{m}{2\pi k_B T}}$$

$$D = \frac{m\lambda^2}{2k_B T}$$

$$E = f_0$$

Thus, we can immediately extract the incoming intensity I_0, the intensity slope ΔI, and the resonant frequency f_0 (or in our case, deviation from resonance). Since our C parameter has two unknowns (T and n_{Sr}), but D has only T, we can solve for T using D, and plug that back into C to get n_{Sr}.